Earth greening mitigates hot temperature extremes despite the effect being dampened by rising CO2

Jie Wu, Yu Feng, Laurent Z.X. Li, Philippe Ciais, Shilong Piao, Anping Chen, Zhenzhong Zeng

Wu, J., et al. (2024). Earth greening mitigates hot temperature extremes despite the effect being dampened by rising CO2. One Earth, 7(1), 100-109. https://doi.org/10.1016/j.oneear.2023.12.003

Earth greening mitigates hot temperature extremes despite the effect being dampened by rising CO_2

Jie Wu[1,2,3,8], Yu Feng[1,3,4,8], Laurent Z.X. Li[5], Philippe Ciais[4], Shilong Piao[6], Anping Chen[7], Zhenzhong Zeng[1,3,9*]

[1] School of Environmental Science and Engineering, Southern University of Science and Technology, Shenzhen 518055, China

[2] Department of Geoscience and Natural Resource Management, University of Copenhagen, Copenhagen, Denmark

[3] Ningbo Institute of Digital Twin, Eastern Institute for Advanced Study, Ningbo 315200, China

[4] Laboratoire des Sciences du Climat et de l'Environnement, UMR 1572 CEA-CNRS-UVSQ, 91191 Gif-sur-Yvette, France

[5] Laboratoire de Météorologie Dynamique, Centre National de la Recherche Scientifique, Sorbonne Université, Ecole Normale Supérieure, Ecole Polytechnique, Paris, France

[6] Sino-French Institute for Earth System Science, College of Urban and Environmental Sciences, Peking University, Beijing, China

[7] Department of Biology, Colorado State University, Fort Collins, Colorado, USA

[8] These authors contributed equally: Jie Wu, Yu Feng

[9] Lead contact

*Correspondence: zengzz@sustech.edu.cn

November 19, 2023

SUMMARY

The escalating threat of climate-induced hot temperature extremes poses a global sustainability challenge impacting ecosystems and public health. While the enhancement of leaf area index (LAI; aka Earth greening) is known to cool global mean air temperature, knowledge gaps exist in its mitigation effect on hot temperature extremes, particularly under rising CO_2 during the past three decades. Our study combining coupled land-atmosphere climate model (IPSL-CM) simulations with global observations suggests that Earth greening has reduced hot days frequency index (TX90p) and warm nights frequency index (TN90p) by -0.26±0.10 days decade^{-1} and -0.38±0.11 days decades^{-1}, respectively, offsetting 4.7% and 5.8% of observed trends globally. However, rising CO_2 levels partly diminished these mitigation effects, without which Earth greening might have offset 7.7% of TX90p and 10.0% of TN90p. Our findings illuminate Earth greening's potential to mitigate hot temperature extremes, offering a pathway towards more resilient and sustainable climate adaptation and mitigation.

Keywords: leaf area index; extreme climate; evapotranspiration; earth system model; climate change mitigation; elevated CO_2 concentration

INTRODUCTION

Hot temperature extremes can cause pervasive and detrimental impacts on ecosystems and human society[1], such as reduced carbon sink[2], increased wildfires[3], and higher human morbidity and mortality[4]. With global warming, the frequency and intensity of hot temperature extremes are expected to increase[5], highlighting the importance of finding effective solutions to reduce or avoid the impacts of hot temperature extremes. While the increase in temperature extremes is often associated with or modulated by changes in large-scale meteorological patterns[6,7], land-atmosphere feedback[8,9], and local and regional forcings such as land use and land cover changes[10,11], green vegetation usually can cool air temperature, especially at low- and mid-latitudes[12]. During the past 30 years, the vegetation leaf area index (LAI) has increased across the globe (Figure S1), a phenomenon known as Earth greening[13]. This greening trend regulates the redistribution of heat and moisture at local to regional and global scales by increasing carbon sink and modifying biogeophysical energy exchanges between the atmosphere and the land surface[14].

Prior studies have extensively documented the mitigation effect of Earth greening on *mean* (surface air/land surface) temperatures during the past years, investigated based on long-term remote sensing observations[15] or global climate models[16]. Yet, both offline modeling (e.g., satellite observations) and coupled modeling have failed to address the question of how Earth greening reshapes the occurrence of daytime and nighttime temperature extremes, hindering insights for adaptation strategies and risk assessment, and efforts to mitigate the potentially devastating consequences of climate change on ecosystems and human well-being. Furthermore, prior offline modeling studies struggled to separate the impacts of the concomitant increase in atmospheric CO_2 concentration ($[CO_2]$), whose radiative forcing and physiological effect[17] makes the net effects of greening on hot temperature extremes even more complex. When CO_2 serves as a greenhouse gas within the atmosphere, the radiative forcing heats the land and the warming lead to an increase in vapor pressure deficit that increases evapotranspiration (ET). On the other hand, the physiological forcing of CO_2 reduces plant stomatal openness under high $[CO_2]$ and thus limits plant transpiration (E_t) and associated evaporative cooling[18,19]. Recent research implies that CO_2 physiological forcing may amplify projected regional and global warming[19,20]; some also attribute the future amplification of heat extremes to CO_2 vegetation forcing[17,21]. Yet these studies focus on the projected effects of elevated $[CO_2]$ within CMIP simulations, where the $[CO_2]$ increases at a rate of 1% per year till a quadrupling to 1,132 parts per million (ppm) over 140 years. Knowledge gaps exist in how the rising $[CO_2]$ during the past three decades affected the ΔLAI-induced climatic effects, the study of which aids in refining climate strategies, advancing predictive models, and enhancing understanding of Earth's climate dynamics for more effective, sustainable management.

Here we quantify how Earth greening affects hot temperature extremes under rising $[CO_2]$ by combining time-evolving (i.e., transient) Atmospheric Model Intercomparison Project (AMIP) simulations (Table S1) with global observations. We find that Earth greening during the past 30 years has significantly reduced the frequency of hot days (TX90p) and warm nights (TN90p) globally, at rates of -0.26±0.10 days decade^{-1} and -0.38±0.11 days decade^{-1}, respectively, offsetting 4.7% and 5.8% of the observed trends in TX90p and TN90p during the study period. These mitigation effects are partly dampened by rising $[CO_2]$, without which the mitigation effects could reach -0.43±0.12 days decades^{-1} for TX90p and -0.65±0.17 days decades^{-1} for TN90p, offsetting 7.7% and 10.0% of the observed trends. Our study fills the knowledge gap by demonstrating Earth greening's substantial role in mitigating hot temperature extremes globally, which offers crucial

insights for policymakers and practitioners, enabling the development of targeted strategies for climate adaptation and mitigation. By acknowledging the nuanced regional impacts, our results can inform localized interventions to manage hot temperature extremes, contributing to a more resilient and sustainable future.

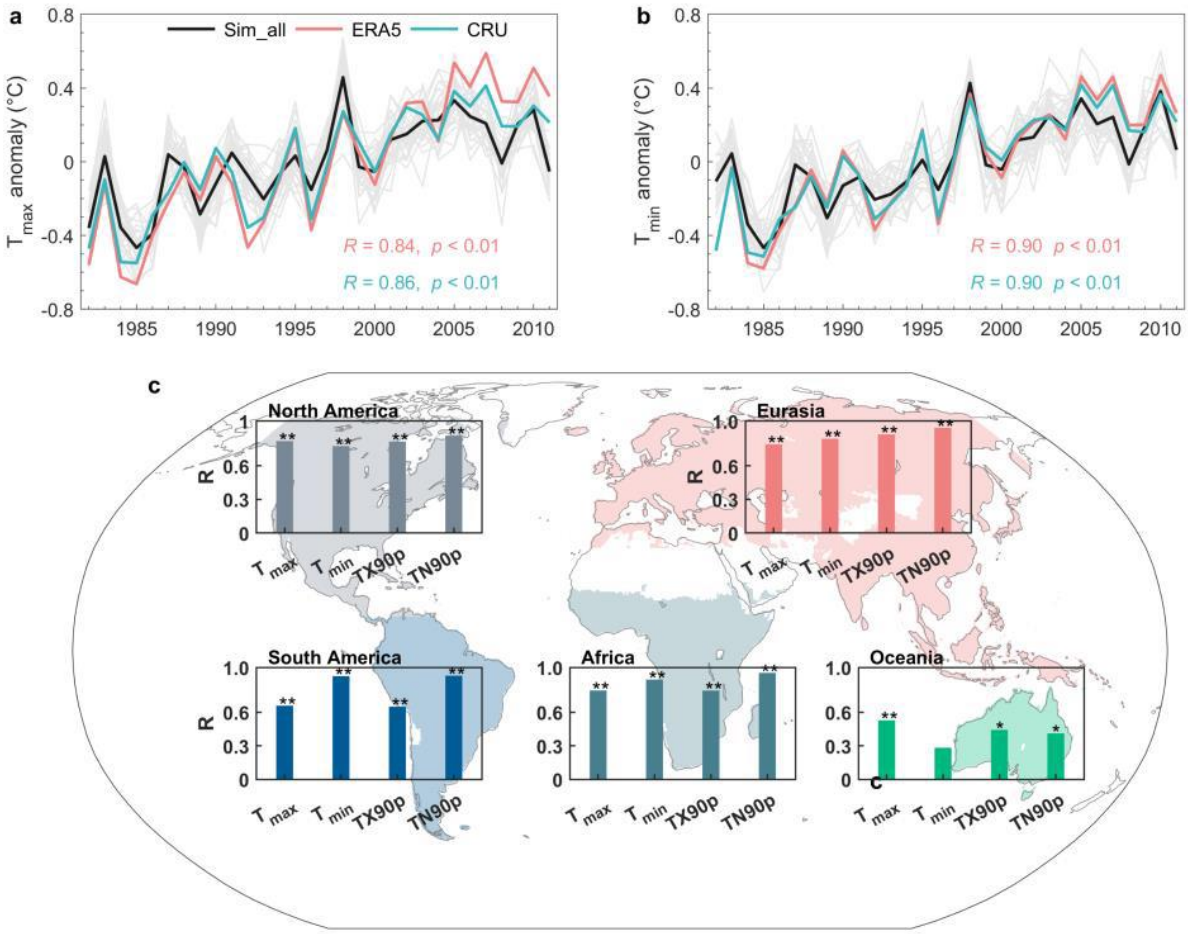

Figure. 1. The capacity of IPSL-CM4 to reproduce observed maximum and minimum air temperature and hot temperature extremes. (**A** and **B**) Interannual anomalies of the globally area-weighted average of the observed and simulated (**A**) maximum air temperature (T_{max}) and (**B**) minimum air temperature (T_{min}) from 1982 to 2011. Observed data are from CRU and ERA5. (**C**) Correlation coefficients and the significance level between observed and simulated temperature and hot temperature extremes. TX90p and TN90p are calculated based on the 30-yr ERA5 daily T_{max} and T_{min}. The simulated data were from the experiment SIM_LAI. Different subregions are masked by different colors. **, $P < 0.01$; *, $P < 0.05$.

RESULTS

Methods Summary

We quantify the climatic effects of Earth greening on hot temperature extremes and separate the influences of rising [CO_2] by performing two pairs of transient AMIP simulations (EXP1 and EXP2; Table S1). EXP1 consists of a control experiment (abbreviated as CTRL) and SIM_LAI. Both simulations were run for 30 years and constrained by the same observational sea surface temperatures (SSTs), sea ice coverage (SIC), and atmospheric [CO_2] between 1982-2011, yet with

different prescribed LAI. In the CTRL, seasonal LAI curves, predicted from multi-decadal averaged monthly climatology, were fixed across different years during the study period. SIM_LAI was prescribed with satellite-observed monthly LAI that varies annually. The difference between SIM_LAI and CTRL reflects the response of the Earth system to the observed LAI change (referred to as ΔLAI) under rising [CO_2]. To investigate the effects of rising [CO_2], we performed an additional EXP2 in which [CO_2] is fixed to be 341 ppm (the [CO_2] 1982's level). The indices we used to represent hot temperature extremes are the hot days frequency index (TX90p) and the warm nights frequency index (TN90p) recommended by the Expert Team on Climate Change Detection and Indices[22]. Both TX90p and TN90p are percentile-based indices quantifying the exceedance rates (in %) of days with daily maximal/minimal air temperatures (T_{max}/T_{min}) above the 90th percentile of a base period, allowing for comparability across different climatic regions that cannot be done with threshold-based indices[23] (more details refer to *Experimental Procedures*).

We first conducted a rigorous evaluation on the capability of IPSL-CM4 in representing the climate effects of LAI changes and rising [CO_2], based on its proven good performance in estimating temperature, precipitation, evapotranspiration, and soil moisture in previous studies[24,25,26]. The model simulation for comparison was SIM_LAI, as it was constrained by realistic SST, SIC, [CO_2] and LAI, thus closest to the historical climate. We found that the spatial pattern of the simulated multi-year average monthly T_{max}, $T_{min,}$ and precipitation are in strong agreement with Climate Research Unit (CRU) observed patterns, with spatial correlation coefficient (R) of 0.99, 0.97, and 0.70, respectively (all with $P < 0.01$; Figures S2, S3 and S4). Additionally, the comparison against CRU and ERA5-Land reanalysis surface air temperature showed that the modeled area-weighted global average of T_{max} and T_{min} are significantly and highly correlated with observations at temporal variation, with R of 0.84 (CRU) and 0.86 (ERA5) for T_{max} ($P < 0.01$, Figure 1A) and R of 0.87 (CRU) and 0.86 (ERA5) for T_{min} ($P<0.01$, Figure 1B). Regionally, the comparisons between the IPSL-CM4 simulated and observation-based T_{max} and T_{min}, as well as the calculated TX90p and TN90p, further demonstrated the model's good performance in estimating hot temperature extremes, especially in North America, Eurasia, and Africa, where the correlation coefficient is as high as 0.952 (Figures 1C and S5).

Effects of ΔLAI on hot temperature extremes

To investigate the effects of Earth greening on hot temperature extremes, we calculated the differences in TX90p and TN90p between SIM_LAI and CTRL. To make the analyses more robust, we used a bootstrapping approach by randomly resampling 80% of the 30 realizations each time and derived the ensemble mean of the 24 realizations. We subsequently repeated the analyses 10,000 times and generated a large sample size of 10,000 (grey lines in Figures 2A, C). The paired GCM analysis showed that, globally, the green-up during 1982–2011 caused a statistically significant decrease in T_{max} and T_{min} ($P < 0.01$), with a decreasing rate of -0.025±0.006 °C decade^{-1} for T_{max} and -0.024±0.005 °C decade^{-1} for T_{min} (Figure S6), which can be translated to -0.26±0.10 days decade^{-1} and -0.38±0.11 days decades^{-1} in TX90p and TN90p, respectively. Among the subregions, Eurasia experienced the most pronounced decline in TX90p (0.52 days decade^{-1}, $P<0.01$) attributable to vegetation greening, followed by North America and South America (inserted box in Figure 2B). In terms of warm nights, greening has caused a reduction in TN90p across all the four continents (inserted box in Figure 2D), with the most significant trend occurring in Eurasia (0.51 days decade^{-1}, $P<0.01$) and Africa (0.50 days decade^{-1}, $P<0.05$).

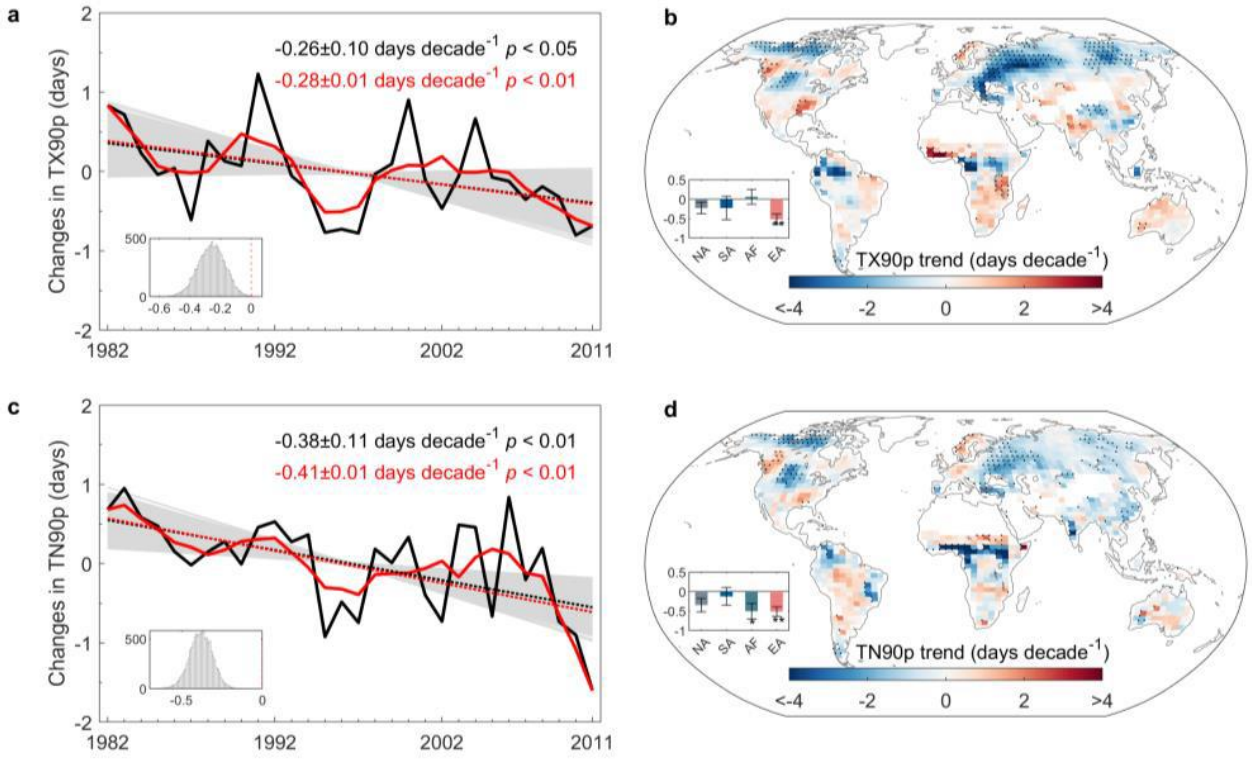

Figure. 2. IPSL-simulated changes in annual hot temperature extremes indices. (**A** and **C**) Interannual anomalies of the globally area-weighted average of (**A**) the hot days frequency index (TX90p) and (**C**) the warm nights frequency index (TN90p) induced by earth greening. The black solid lines are the annual values and the red solid lines are the 5-yr-window moving average. The black dashed line and the red dashed lines are the corresponding regressions. The gray lines are the regressions of the bootstrapped results (randomly resampling an 80% subset of the 30 realizations each time and repeating the analyses 10,000 times). Inserted box shows the frequency distribution of the regression trends derived from the 10,000 resampling results. (**B** and **D**) Spatial pattern of the ΔLAI-induced trends in (**B**)TX90p and (**D**)TN90p. Stippling indicates a significant trend ($P < 0.05$). The inserted box shows the trend of ΔLAI-induced TX90p/TN90p over the four different subregions. NA: North America; SA: South America; AF: Africa; EA: Eurasia. Oceania is excluded for analysis due to the lower correlation coefficients.

Spatially, several general features emerge. First, the patterns of the changes in TX90p and TN90p resemble that of LAI change. The highest rates of TX90p (TN90p) decrease occur mainly in regions with distinct greening, e.g., northern Alaska and Canada, Europe, eastern Siberia, north Amazonia, and tropical rainforest in Central Africa (Figures 2B, D and S1B). In contrast, in regions where LAI decreased significantly (defined as browning), such as the North American boreal forests, TX90p (TN90p) showed a positive trend (Figure 2B, D). A notable exception is Sahel where TX90p and TN90p increased despite the enhanced LAI. By investigating ΔLAI and ΔLAI-induced changes at the seasonal scale, we found that in the Sahel, the observed enhancement of LAI mainly occurs during SON (September, October and November; Figure S1H), whereas LAI decreased significantly in MAM (March, April and May; Figure S1D). The browning in MAM led to an increase in T_{max}/T_{min} (Figures S7B and S8B) and TX90p/TN90p (Figures S9B and S10B), which dominated the TX90p/TN90p increase at the annual scale. The increase in TX90p over eastern Africa could also be explained by the browning in SON. Despite the different responses in certain regions, the spatial coherence between LAI change and its induced TX90p/TN90p trend at different scales provides evidence of the mitigation effects of Earthing greening on hot temperature extremes.

Second, the changes in T_{max}/T_{min} are not representative of TX90p/TN90p. For example, both TX90p and TN90p decreased dramatically over Northern Alaska and Canada whereas the declining trends of T_{max} and T_{min} are not significant (Figure S6B, D).

Seasonally, a greening-induced decline in T_{max} and T_{min} was observed in all the seasons (Figures S7 and S8); yet only in JJA (June, July and August) the change was significant for both TX90p and TN90p (both around 0.22 days decade^{-1}, $P < 0.01$; Figures S9C and S10C). TN90p also decreased in SON and DJF (December, January and February; Figure S10E, G). Besides, the mitigation effect on hot temperature extremes is more pronounced in local summer than in winter, for instance, more in JJA than in DJF for the Northern Hemisphere, and vice versa for the Southern Hemisphere.

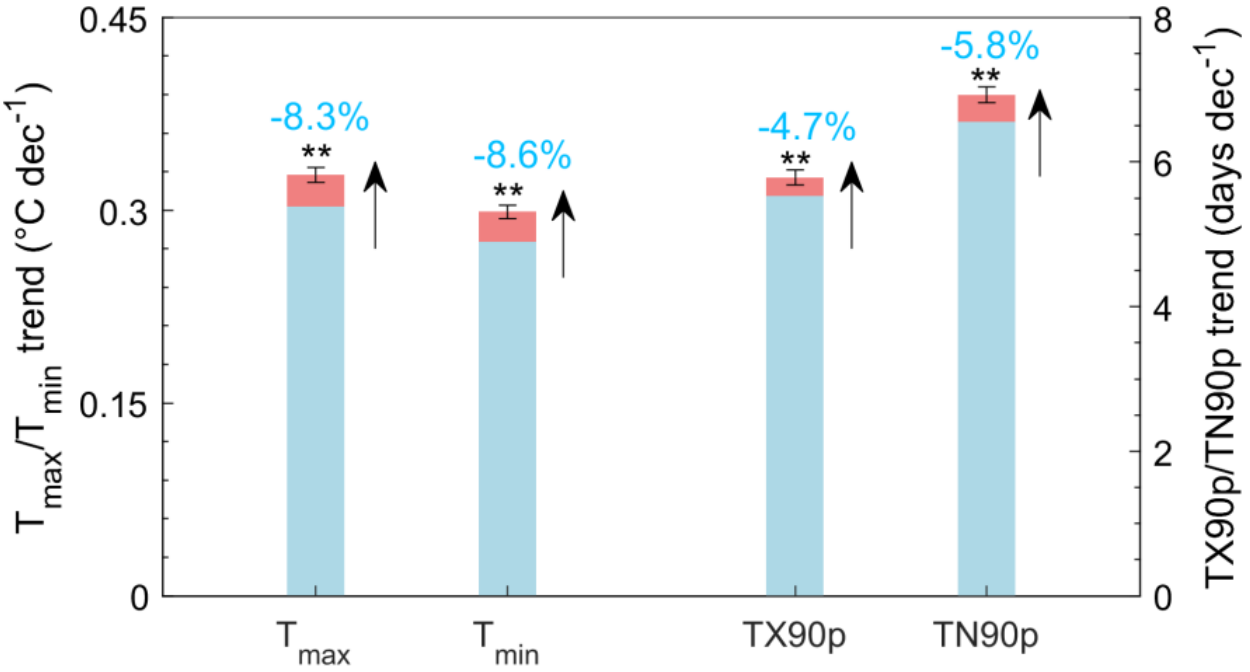

Figure. 3. Greening-induced mitigation effects. Comparison of the observed and ΔLAI-induced changes in T_{max}, T_{min}, hot days frequency index (TX90p) and warm nights frequency index (TN90p) over the globe. The below blue bars are the observed changes and the stacked pink bars are the ΔLAI-induced changes. Note that the trends of ΔLAI-induced changes are negative; the directions are converted to positive for straightforward comparison. The blue numbers are the ratios of the ΔLAI-induced changes to the observed trends. Among the four blue bars, the left two representing the realistic change of T_{max} and T_{min} are computed from CRU and ERA5; the right two are the average of the extreme temperature indices calculated from observation-based data ERA5 and HadEX2. Error bars show a 95% confidence interval. **, $P < 0.01$; *, $P < 0.05$.

Mitigation effects of Earth greening over the past 30 years

To further quantify the mitigation effects of Earth greening on hot temperature extremes, we compared modeled trends of T_{max}, T_{min}, TX90p and TN90p against corresponding observations between 1982 and 2011. Apart from the TX90p and TN90p calculated with the 30-yr daily T_{max} and T_{min} from ERA5, we also used the direct gridded outcome from HadEX2, a global station-based dataset of climate extremes indices[27] (more details refer to *Experimental Procedures*). Globally, observed T_{max} and T_{min} increased at the rate of around 0.3 °C decade^{-1} during the study

period; TX90p and TN90p grew at 5.5 days decade^{-1} and 6.5 days decade^{-1}, respectively, indicating the severe threats of global warming and hot temperature extremes (blue bars in Figure 3). The ΔLAI-induced reduction in T_{max}, T_{min}, TX90p and TN90p offset 8.3%, 8.6%, 4.7% and 5.8% of the observed increasing trend (pink stacked bars in Figure 3), respectively.

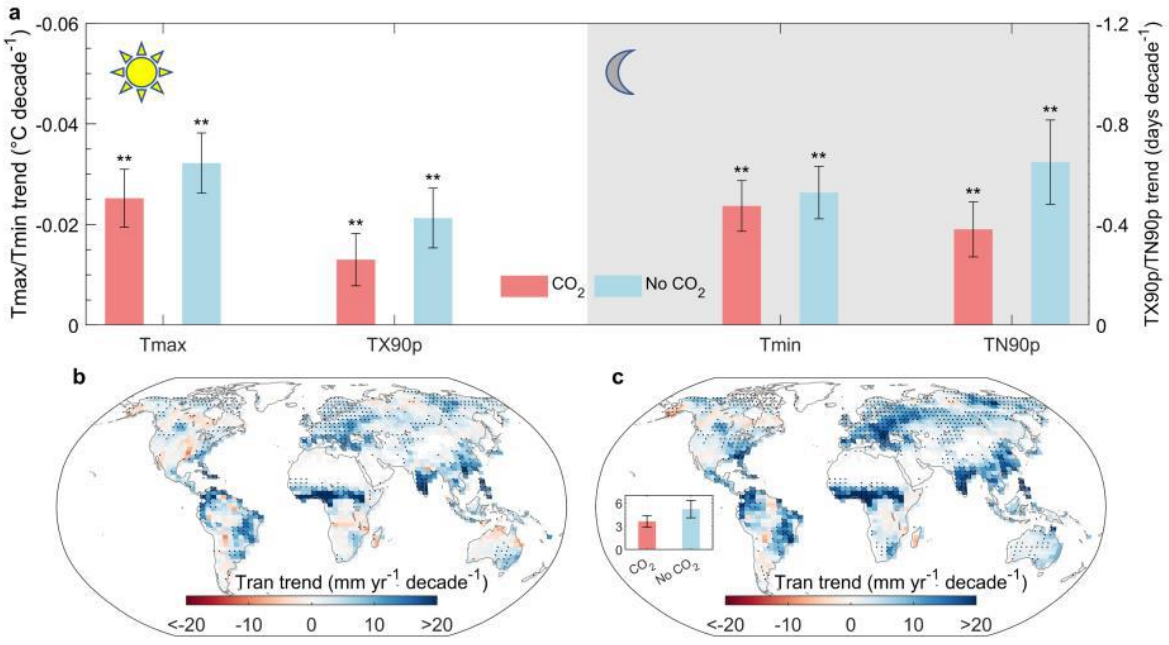

Figure. 4. The effects of rising atmospheric [CO_2]. (A) The comparison between the ΔLAI-induced changes in T_{max}, T_{min}, TX90p and TN90p over the globe with (pink bars) and without (blue bars) CO_2 effects considered. Error bars show a 95% confidence interval. **, P < 0.01; *, P < 0.05. **(B)** Spatial pattern of the ΔLAI-induced trends in transpiration (E_t) under CO_2 effect. Stippling indicates a significant trend (P < 0.05). **(C)** Same as (**B**), but for transpiration without considering CO_2 effect. The inserted box shows the comparison of the trend of ΔLAI-induced transpiration.

Plants influence hot temperature extremes by regulating energy and water exchange between the land and the atmosphere[17]. LAI is closely related to ET, the combined water loss through E_t, canopy interception and soil evaporation. As vegetation cover expands, water loss through E_t increases (Figure 4B), particularly over regions with significant LAI increase (Figure S1B). Despite the potential decrease in soil evaporation, total ET increases in response to Earth greening, considering the dominant role of E_t over ET[28,29]. The enhanced ET plays a crucial role in cooling the Earth's surface and the surrounding atmosphere. As water evaporates, it removes heat energy from the surface, which helps to lower temperatures and reduce hot temperature extremes. Prior research has indicated that the rise in ET is the primary contributor to the ΔLAI-induced cooling impact on *mean* temperature[16]. Our model simulations showed that global ET increased at 2.21±0.54 mm yr^{-1} decade^{-1} (P<0.01; Figure S11). Spatially, ET enhancement occurred in regions with increasing LAI, explaining the reduction in hot temperature extremes in these regions, and vice versa. A typical example of ET decrease is the southeastern US experiencing a notable increase in TX90p and TN90p. Additionally, model simulations showed that Earth greening reduced atmospheric shortwave transmissivity significantly over regions like north Eurasia, contributing to the cooling effects over these regions (Figure S12).

However, it should be noted that some regions including South Asia experienced an increase in TX90p despite the enhanced LAI. After excluding the effects of strong browning in some seasons, we speculate that this TX90p increase was caused by ΔLAI-induced soil moisture change[23,30]. Greening is expected to affect soil moisture content in two opposite ways. On the one hand, enhanced LAI supports the persistence of soil moisture by increasing transpiration to favor more precipitation[31,32]. On the other, greening leads to greater water loss and faster soil moisture depletion[26]. Figure S13 shows that enhanced LAI strongly decreases soil moisture content over eastern America, Sahel, Central Asia, South Asia, Northern China, and Australia, most of which are arid regions. Seasonally, soil moisture content declines more substantially in the drier season. Taking South Asia as an example, both SON and DJF witnessed a substantial increase in LAI, but the responses of soil moisture content are different. During the dry season (DJF), soil moisture content strongly decreases; it only slightly decreases during the wet season (SON). Considering the soil moisture memory[33], soil moisture content could decline at the annual scale over these arid and/or seasonally arid regions. The drying of soil moisture increases sensible heat flux and reduces latent cooling, thereby increasing hot temperatures[34].

Effects of rising CO_2 concentration

When compared against global observations, the simulation SIM_LAI_no_CO_2 has a slightly lower correlation (Figures S14 and S15) than SIM_LAI, demonstrating the role of elevated [CO_2] in accurately diagnosing the climate feedback to Earth greening. The comparison of climate between EXP1 and EXP2 reveals that the effects of rising [CO_2] have greatly reduced the ΔLAI-induced mitigation effect on daily T_{max}/T_{min} and hot temperature extremes (Figure 4A). The dampened mitigation effect is partly due to the CO_2 radiative forcing, which offsets the greening-induced cooling by heating the land surface[5].

In terms of daily temperatures, CO_2 effects act preferentially on T_{max} than T_{min}: when CO_2 is not considered, T_{max} decreased at the rate of -0.032±0.006 ℃ decade^{-1}, 28% faster than that under rising [CO_2]. In contrast, the change in the T_{min} trend is slight. It could be explained by the fact that vegetation photosynthesis primarily occurs during the daytime. In theory, most plant types tend to close their stomata in response to elevated [CO_2], thereby decreasing E_t rates by increasing plant water-use efficiency[35]. By comparing the ΔLAI-induced E_t change in two experiments, we find that global E_t slowed down its increasing pace from 5.22±1.12 mm yr^{-1} decade^{-1} to 3.62±0.76 mm yr^{-1} decade^{-1} ($P<0.01$) when considering the CO_2 effect (inserted box in Figure 4C). In some arid regions including Central America, the trend of E_t even shifted from increase (Figure 4C) to decrease (Figure 4B). This physiologically driven decline in E_t diminished the associated evaporative cooling, thus weakening the cooling effects of enhanced LAI during the daytime. As for hot temperature extremes, the mitigation effects on TX90p and TN90p are dampened by rising [CO_2]. If removing the impact of CO_2, the reduction rates of TX90p and TN90p due solely to the enhanced LAI could reach -0.43±0.12 and -0.65±0.17 days decades^{-1}, respectively, offsetting 7.7% and 10.0% of the observed increase in hot temperature extremes.

DISCUSSION

Recognizing Earth greening's pivotal role in mitigating hot temperature extremes is instrumental in shaping robust strategies for climate change mitigation, fostering resilience, and offering pathways toward more sustainable and resilient environments. Our study showed a reduction in daytime and nighttime temperature and hot temperature extremes induced by Earth greening,

attributed to the higher ET and lower atmospheric shortwave transmissivity. It complements previous studies on *mean* temperature, bridging the knowledge gap in the climatic effects of Earth greening on hot temperature extremes and the effects of rising [CO_2].

A paradox becomes apparent in the context of the nocturnal cooling phenomenon, wherein nighttime ET rates are generally low, and an increase in LAI would likely yield only a marginal rise in ET, which proves inadequate in generating a substantial mitigating influence during the nighttime period. A plausible explanation lies in the reduction in aerodynamic resistance. Earth greening reduces aerodynamic resistance due to an increase in surface roughness[36], which enhances the flow of sensible heat from the warmer ground to the cooler atmosphere during nighttime. By facilitating this heat transfer at night, the reduced aerodynamic resistance from Earth greening helps cool down the Earth's surface during the night. The legacy effects of daytime cooling may also contribute to the nighttime cooling. Notably, surface air temperature decreases in response to Earth greening during daytime, subsequently leading to a decline in ambient air temperature after sunset. Examining the simulated diurnal variation of the ΔLAI-induced cooling effects, we observed a consistent decrease in surface air temperature throughout the day, with a more pronounced reduction during daytime than at nighttime (Figure S16B). Spatially, the high and significant spatial correlation between the T_{max} and T_{min} trend at the grid scale further demonstrated the relationship between daytime and nighttime cooling ($R=0.74$, $p<0.01$; Figure S16A). This correlation implies that regions experiencing daytime cooling also undergo concurrent nighttime cooling. The slope of the regression line also indicated a greater magnitude of daytime cooling relative to its nighttime counterpart. Another potential contributor is the alterations in the soil heat flux. A precedent study by Yu et al.[37] attributed the greening-induced nighttime cooling impact on land surface temperature (T_s) to the feedback from soil heat flux. Our model simulations revealed a pronounced decline in soil heat flux in response to Earth greening, with a decreasing rate at 0.22 ± 0.06 W m^{-2} $decade^{-1}$ globally ($P<0.01$; Figure S17), which would reduce T_s. Considering the relationship between T_s and T_a[38], such a decrease in soil heat flux likely exerts negative feedback on nocturnal air temperature, leading to a significant nighttime cooling effect.

The greening-induced cooling effects and the reduction in hot temperature extremes have important implications for adaptation strategies to climate change. The 4.7% and 5.8% mitigation effects on hot temperature extremes are substantial because any small increase in hot temperature extremes would be disproportionally detrimental to human health and biodiversity[39]. Hot extremes contribute to higher morbidity and mortality during heat waves[4,40]. Based on a map of global population densities[41], we roughly estimated that the cooling effects with significant trends ($P<0.05$) induced by the past greening have benefited billions of people. Specifically, greening has significantly reduced TX90p for 0.6 billion people, particularly in African countries near the Gulf of Guinea and Europe which were hotspots of recent heat waves (Figure S18). Around 1.0 billion people have benefited from ΔLAI-induced significant reduction in TN90p ($P<0.05$), mainly located in Europe, China, India, and African countries near the equator. It is especially noteworthy to highlight the greening-induced mitigation effects for low-income countries near the equator. Living under hot temperatures close to the upper threshold for human comfort for most of a year, people in these regions also experienced more hot temperature extremes, as even a small increase in temperature would trigger a new hot extreme due to the naturally narrow temperature variability[42]. In addition, these regions also have limited resources, such as air conditioning. Thus, these low-income countries are particularly vulnerable to global warming and the associated hot temperature extremes. Our results show that greening-induced cooling effects and the reduction in hot temperature extremes provide a nature-based solution to help mitigate adverse climate change impacts in low-

income countries. Besides human health benefits, Earth greening-induced mitigation of hot extremes also provides ecosystem benefits, which can be manifested in two aspects. First, the cooling effect reduces the frequency of hot extreme events during which acute thermal stress can damage or kill organisms. Second, the regions with the greatest numbers of species exposed are often areas experiencing a reduction in hot temperature extremes. For example, the most substantial decrease in TN90p occurred in tropical regions, where the diversity peaked for species such as ant genera, amphibians, birds, and mammals[43].

Notwithstanding, our beneficiary population estimation bears uncertainties due to the coarse spatial resolution and the absence of an integrated urban module in IPSL-CM. The spatial resolution of IPSL-CM is 2.5° latitude by 3.75° longitude, which would be beyond the scope and extent of the ΔLAI-induced mitigation effects. As a result, counting all the population within a pixel as the beneficiary population would lead to an overestimation. However, analogous to the forest loss in Brazil, whose resultant warming impact extends beyond local confines to regions within 50 kilometers[44], Earth greening similarly engenders climate effects through teleconnections, in addition to the local cooling effects. An illustrative case comes from the findings of Lian et al.[26], who uncovered the transportation of extra moisture from Europe to central Siberia. Another uncertainty comes from the omission of the urban module within IPSL-CM. Urban areas accommodate large population, and typically have higher temperatures due to the urban heat island effect. Previous research showed that urban greening can alleviate the impacts of extreme heat exposure on human populations[45]. The absence of an urban model poses challenges in accurately representing the complexities of urban environments and investigating the interactions between LAI change and overall urban microclimate.

Additionally, our study quantified the effects of rising CO_2 in modulating the climatic response to Earth greening during the past decades, which is of great importance for feedback loops study, policy and mitigation strategies, and risk assessment and adaptation. Yet the discrete disentanglement of the influences attributed to radiative and physiological CO_2 effects is lacking due to the scope of our study design. As such, our analysis presently provides an aggregate quantification of the cumulative impacts arising from these two effects. Furthermore, the capacity of the IPSL-CM model to faithfully replicate real-world CO_2 effects is subject to uncertainty. Land surface models usually relate stomatal conductance, a measurement of the degree of stomatal opening, to photosynthesis via semi-empirical formulations[46] and related theoretical models[47,48]. The stomatal conductance model used in the ORCHIDEE of IPSL-CM is the Ball-Berry conductance model. While widely utilized, this model simplifies the intricate relationship between stomatal conductance and the net assimilation rate of carbon dioxide, overlooking potential nonlinearities and variations in physiological responses under diverse conditions. As a result, the model might not fully capture the nuanced complexities of stomatal behavior and its interactions with rising atmospheric CO_2 concentrations. This underscores the necessity for validation against observations and continuous refinement to enhance the model's accuracy in representing stomatal responses and associated CO_2 effects.

In summary, this study has advanced our understanding of how the enhanced vegetation activity has affected hot temperature extremes over the vegetated land during the past decades. Although dampened by the effects of rising [CO_2], the greening substantially mitigated the observed hot temperature extremes that are disproportionally detrimental to human health and biodiversity. Billions of people, particularly those living in low-income countries near the equator, are estimated

to benefit from the greening-induced cooling effects and the reduction in hot temperature extremes, highlighting the contribution of the nature-based solution in mitigating adverse climate change impacts.

EXPERIMENTAL PROCEDURES

Resource availability

Lead contact

Further information and requests for resources should be directed to and will be fulfilled by the lead contact, Zhenzhong Zeng (zengzz@sustech.edu.cn).

Materials availability

Not applicable to this study.

Data and code availability

The monthly sea surface temperature and sea ice coverage data are available at https://esgf-node.llnl.gov/news/list/input4mips/). CRU monthly air temperature data are available at https://crudata.uea.ac.uk/cru/data/hrg/; ERA5 hourly air temperature data are available at https://cds.climate.copernicus.eu/; HadEX2 data are available at https://climatedataguide.ucar.edu/climate-data/hadex2-gridded-temperature-and-precipitation-climate-extremes-indices-climdex-data; The Gridded Population of the World (v4) is available at https://sedac.ciesin.columbia.edu/data/collection/gpw-v4. IPSLCM GCM model code is available at http://forge.ipsl.jussieu.fr/igcmg/svn/modipsl/trunk. The scripts used to generate all the results are MATLAB (R2020a). Analysis scripts are available on request from Z. Zeng.

Experimental setup and model

To investigate the effects of Earth greening on hot temperature extremes, we performed a pair of transient Atmospheric Model Intercomparison Project (AMIP) simulations, a framework for conducting numerical experiments using atmospheric models that are prescribed with the observed sea surface temperatures (SSTs) as input to the model, without allowing the model to simulate its own ocean interactions. By doing so, AMIP simulations could reduce the uncertainty caused by errors in ocean dynamics, the main contributor to the systematic biases in the climatology in fully coupled climate models [49,50].

In our AMIP-like simulations, we coupled the atmospheric and the land surface models of IPSL-CM (version 4). IPSL-CM is developed by the Institute Pierre Simon Laplace (IPSL) modeling community[50]. Its atmospheric model is Laboratoire de Météorologie Dynamique atmospheric general circulation model with Zooming capability[52] (LMDZ), which has been successfully applied to investigate climate studies like how advection affect surface air temperature (Cauquoin et al., 2019). The land surface component is ORCHIDEE[53] (Organising Carbon and Hydrology In Dynamic Ecosystems). ILSL-CM has proven its capability in simulating temperature, precipitation, evapotranspiration, and soil moisture[24,25,26]. The model resolution was 2.5° latitude × 3.75° longitude, with 19 vertical levels and a 3-minute time step.

After controlling SSTs and sea ice boundary conditions, we could isolate the response of the atmospheric component of climate models to Earth greening and [CO_2] by conducting two sets of experiments (EXP1 and EXP2; see Supplementary Table 1). EXP1 consists of a control experiment (abbreviated as CTRL) and SIM_LAI. Both simulations were run for 30 years and constrained by observational SSTs, sea ice coverage (SIC), and atmospheric CO_2 concentration during the study

period. The only difference is the LAI conditions prescribed, the proxy characterizing vegetation greenness. In CTRL, LAI was fixed as the monthly varying climatology during the period 1982 to 2011. The climatological LAI maps lost the feature of year-to-year variation and trend. SIM_LAI was prescribed with the satellite-observed monthly LAI that varies yearly. The difference between SIM_LAI and CTRL (SIM_LAI minus CTRL) demonstrates the Earth system's climatic response to increased LAI and atmospheric CO_2 concentration.

To investigate how rising atmospheric CO_2 affects the climatic effects of increased LAI on hot temperature extremes, we performed EXP2 with a group of transient simulations in which CO_2 concentration is set to be 341 ppm (parts per million; the CO_2 concentration at 1982's level). Except for CO_2 concentration, the two experiments in EXP2 share the same configurations as those in EXP1: SIM_LAI_no_CO_2 corresponds to SIM_LAI with the same observational SST, SIC, and LAI but different CO_2 concentrations; CTRL_no_CO_2 corresponds to CTRL. The difference between SIM_LAI_no_CO_2 and CTRL_no_CO_2 runs reveals the simulated climatic response due solely to increasing LAI. The comparison between EXP2 and EXP1 isolates the potential effect of rising atmospheric CO_2 on the LAI-climate feedback.

The simulations were performed at the National Computer Center IDRIS, France. All the experiments consist of 30 realizations that started with different initial conditions. To make the analyses more robust, we used a bootstrapping approach by randomly resampling 80% of the 30 realizations each time and derive the ensemble mean of the 24 realizations. We subsequently repeated the analyses 10,000 times and generated a large sample size of 10,000. The analysis was restricted to vegetated regions with a multi-year (1982–2011) mean LAI greater than 0.1.

Data sources

Observational and reanalysis data

We constrained the IPSL-CM4 with observational LAI, SSTs, SIC, and CO_2, all covering the period 1982-2011. The satellite-observed monthly LAI was derived from the Global Inventory Monitoring and Modeling Studies (GIMMS) LAI3g[13]. This dataset has proven good performance in capturing LAI dynamics in various studies[14,26]. We modified ORCHIDEE by substituting LAI with observed values from satellite data at individual grid points and for distinct plant functional types (PFT). This integration process involved utilizing the inherent high spatial resolution of satellite-derived LAI and land-cover data (less than 1 km) to compute averages for allocation onto the model grid. The monthly maps of the SST and SIC were from the AMIP.

Besides the forcing data, a range of observation-based datasets was used to evaluate the model performance and estimate the mitigation effect of earth greening. We use two air temperature datasets, i.e., observational Climatic Research Unit (CRU) air temperature product and ERA5 reanalysis air temperature product. CRU (version 4.05, CRU TSv4.05) is a widely used observed climate dataset[54], providing gridded monthly maximum 2 m air temperature (T_{max}) and minimum 2 m air temperature (T_{min}) at a 0.5° resolution for the period 1901 to 2020 across the globe's land surface except for Antarctica. The gridded variables are derived by interpolating monthly anomaly fields converted from each station series. ERA5 is the latest generation of reanalysis data created by the European Centre for Medium-Range Weather Forecasts (ECMWF); it provides 2m air temperature at higher spatial (~0.25°) and temporal resolution (hourly), potentially making it suitable to estimate the climate extremes[55]. We used both ERA5 and CRU data in terms of air temperature (T_{max} and T_{min}) simulation assessment but only used ERA5 daily temperature

(calculated from hourly T_{max} and T_{min}) for hot temperature extremes evaluation, as CRU does not provide daily data.

Apart from calculating the extreme temperature indices from observation- and reanalysis-based data, we also used the gridded outcome of HadEX2, a global station-based dataset of climate extremes indices[27]. HadEX2 provides 17 temperature and 12 precipitation indices spanning 1901–2010 at monthly and annual time steps. These indices are calculated based on high-quality in situ observations of daily T_{max}, T_{min} and precipitation, following consistent definitions recommended by the Expert Team on Climate Change Detection and Indices (ETTCCDI). As for extreme temperature indices, approximately 7,000 temperature meteorological stations globally are included. The indices are first computed at each station over the period of record available and then grided to a 2.5° latitude by a 3.75° longitude grid.

Indices of extreme hot temperatures

We used two ETCCDI indices, i.e., the hot days frequency index (TX90p) and the warm nights frequency index (TN90p), to measure the modeled changes in hot temperature extremes[22]. TX90p and TN90p quantify the exceedance rates (in %) of days with daily T_{max}/T_{min} above the 90^{th} percentile of a base period. The percentiles were calculated for each calendar day centered on a 5-day sliding window for the base period. Different from the ETCCDI indices which define the base period as 1961-1990, we calculated the percentiles based on all days of the 30-yr study period following previous studies[56]. We also converted TX90p and TN90p to days by multiplying the probability (in %) by the number of days in the year.

Global population data

We used the Gridded Population of the World (the fourth version) to quantify the distribution of the global human population count for the year 2010 (ref. [41]). The data at 5 km resolution were further resampled to 2.5° latitude × 3.75° longitude resolution by summing all the 5 km pixels, to match the resolution of IPSL-CM4 outputs.

Caveats and Limitations

This study has advanced our understanding of how the enhancement of leaf area over vegetated land during the past 30 years has affected hot temperature extremes at the global scale. However, caveats and limitations remain. In addition to the abovementioned uncertainties in the main text, using a single ESM may be subject to model dependence. ESMs incorporate diverse parameterization schemes for processes such as radiation, cumulus convection, turbulence, cloud microphysics, and land surface interactions, leading to potential discrepancies in model simulation outputs. To address this concern, we sought to enhance the credibility by choosing the ESM with greater capability and conducting vigorous validation against observations. IPSL-CM has exhibited advantages in simulating the sensitivities of albedo and ET to LAI compared to other ESMs, such as the Community Earth System Model (CESM) and the Australian Community Climate and Earth System Simulator coupled model (ACCESS)[16]. We also conducted rigorous evaluations on the model's capability in simulating climate effects. Moreover, constrained by the somewhat coarse spatial resolution of our model, although PFT data provides the percentage of each land cover, it does not fully depict the degree of LAI change and the resulting cooling impacts associated with each land cover category. This issue holds significant scientific implications for understanding climate mitigation within diverse ecosystems. Future research endeavors that integrate high-resolution Earth system modeling with satellite observations have the potential to yield richer

insights, thereby enhancing our understanding of nature-based solutions to counteract the detrimental impacts of climate change. It should be noted that although subject to considerable uncertainties, these state-of-the-art ESMs represent the highest level of climate simulation. Efforts are desirable to improve the representation of the Earth system so that we can better understand the vegetation-soil moisture-climate feedback.

Supplemental information description

Table S1
Figures S1 to S18

Acknowledgements

This study was supported by the National Natural Science Foundation of China (grants no. 42071022) and the start-up fund provided by Southern University of Science and Technology (no. 29/Y01296122). We thank National Computer Center IDRIS for providing computing resources. We thank OpenAI's DALL-E, a deep learning model for image creation, for creating the background image of graphic abstract.

Author Contributions

Z.Z., L.L., and S.P. designed the research; L.L. performed numerical simulations; Y.F. and J.W. performed the analysis; J.W. wrote the draft. All authors contributed to the interpretation of the results and the writing of the paper.

Declaration of Interests

The authors declare no competing interests.

References

1. Easterling, D. R., Meehl, G. A., Parmesan, C., Changnon, S. A., Karl, T. R., and Mearns, L. O. (2000). Climate extremes: observations, modeling, and impacts. Science *289*, 2068-2074. 10.1126/science.289.5487.2068.
2. Piao, S., Zhang, X., Chen, A., Liu, Q., Lian, X., Wang, X., Peng, S., and Wu, X. (2019). The impacts of climate extremes on the terrestrial carbon cycle: A review. Sci. China Earth Sci. *62*, 1551-1563. https://doi.org/10.1007/s11430-018-9363-5.
3. Guion, A., Turquety, S., Polcher, J., Pennel, R., Bastin, S., and Arsouze, T. (2022). Droughts and heatwaves in the Western Mediterranean: impact on vegetation and wildfires using the coupled WRF-ORCHIDEE regional model (RegIPSL). Clim. Dyn. *58*(9-10), 2881-2903. https://doi.org/10.1007/s00382-021-05938-y.
4. Ebi, K.L., Capon, A., Berry, P., Broderick, C., de Dear, R., Havenith, G., Honda, Y., Kovats, R.S., Ma, W., Malik, A. and Morris, N.B., et al. (2021). Hot weather and heat extremes: health risks. The Lancet *398*(10301), 698-708. https://doi.org/10.1016/S0140-6736(21)01208-3.
5. Masson-Delmotte, V., Zhai, P., Pirani, A., Connors, S.L., Péan, C., Berger, S., Caud, N., Chen, Y., Goldfarb, L., Gomis, M.I. and Huang, M. (2021). Climate change 2021: the physical science basis. Contribution of Working Group I to the Sixth Assessment Report of the Intergovernmental Panel on Climate Change (Cambridge University Press).
6. Loikith, P.C., Waliser, D.E., Lee, H., Neelin, J.D., Lintner, B.R., McGinnis, S., Mearns, L.O. and Kim, J. (2015). Evaluation of large-scale meteorological patterns associated with temperature extremes in the NARCCAP regional climate model simulations. Clim. Dyn. *45*, 3257-3274. https://doi.org/10.1007/s00382-015-2537-x.
7. Schaller, N., Sillmann, J., Anstey, J., Fischer, E. M., Grams, C. M., and Russo, S. (2018). Influence of blocking on Northern European and Western Russian heatwaves in large climate model ensembles. Environ. Res. Lett. *13*(5), 054015. 10.1088/1748-9326/aaba55.
8. Lorenz, R., Argüeso, D., Donat, M.G., Pitman, A.J., van den Hurk, B., Berg, A., Lawrence, D.M., Chéruy, F., Ducharne, A., Hagemann, S. and Meier, A. (2016) Influence of land-atmosphere feedbacks on temperature and precipitation extremes in the GLACE-CMIP5 ensemble. J. Geophys. Res.: Atmos. *121*(2), 607-623. https://doi.org/10.1002/2015JD024053.
9. Vogel, M. M., Zscheischler, J., and Seneviratne, S. I. (2018). Varying soil moisture–atmosphere feedbacks explain divergent temperature extremes and precipitation projections in central Europe. Earth Syst. Dyn. *9*(3), 1107-1125. https://doi.org/10.5194/esd-9-1107-2018.
10. Lejeune, Q., Davin, E. L., Gudmundsson, L., Winckler, J., and Seneviratne, S. I. (2018). Historical deforestation locally increased the intensity of hot days in northern mid-latitudes. Nat. Clim. Change. *8*(5), 386-390. https://doi.org/10.1038/s41558-018-0131-z.
11. Thiery, W., Visser, A.J., Fischer, E.M., Hauser, M., Hirsch, A.L., Lawrence, D.M., Lejeune, Q., Davin, E.L. and Seneviratne, S.I., (2020). Warming of hot extremes alleviated by expanding irrigation. Nat. Commun. *11*(1), 290. https://doi.org/10.1038/s41467-019-14075-4.
12. Alkama, R., Forzieri, G., Duveiller, G., Grassi, G., Liang, S., and Cescatti, A. (2022). Vegetation-based climate mitigation in a warmer and greener World. Nat. Commun. 13(1), *606*. https://doi.org/10.1038/s41467-022-28305-9.
13. Zhu, Z., Piao, S., Myneni, R.B., Huang, M., Zeng, Z., Canadell, J.G., Ciais, P., Sitch, S., Friedlingstein, P., Arneth, A. and Cao, C. (2016). Greening of the Earth and its drivers. Nat. Clim. Change. *6*(8), 791-795. https://doi.org/10.1038/nclimate3004.
14. Piao, S., Wang, X., Park, T., Chen, C., Lian, X.U., He, Y., Bjerke, J.W., Chen, A., Ciais, P., Tømmervik, H. and Nemani, R.R. (2020). Characteristics, drivers and feedbacks of global greening. Nat. Rev. Earth Environ. *1*(1), 14-27. https://doi.org/10.1038/s43017-019-0001-x.

15. Li, Y., Li, Z.L., Wu, H., Zhou, C., Liu, X., Leng, P., Yang, P., Wu, W., Tang, R., Shang, G.F. and Ma, L. (2023). Biophysical impacts of earth greening can substantially mitigate regional land surface temperature warming. Nat Commun. *14*(1), 121. https://doi.org/10.1038/s41467-023-35799-4.
16. Zeng, Z., Piao, S., Li, L.Z., Zhou, L., Ciais, P., Wang, T., Li, Y., Lian, X.U., Wood, E.F., Friedlingstein, P. and Mao, J. (2017). Climate mitigation from vegetation biophysical feedbacks during the past three decades. Nat. Clim. Chang. *7*(6), 432-436. https://doi.org/10.1038/nclimate3299.
17. Skinner, C. B., Poulsen, C. J., and Mankin, J. S. (2018). Amplification of heat extremes by plant CO_2 physiological forcing. Nat. Commun. *9*(1), 1094. https://doi.org/10.1038/s41467-018-03472-w.
18. Zarakas, C. M., Swann, A. L., Laguë, M. M., Armour, K. C., and Randerson, J. T. (2020). Plant physiology increases the magnitude and spread of the transient climate response to CO_2 in CMIP6 Earth system models. J. Clim. *33*(19), 8561-8578. https://doi.org/10.1175/JCLI-D-20-0078.1.
19. He, M., Piao, S., Huntingford, C., Xu, H., Wang, X., Bastos, A., Cui, J. and Gasser, T. (2022). Amplified warming from physiological responses to carbon dioxide reduces the potential of vegetation for climate change mitigation. Commun. Earth Environ. *3*(1), 160. https://doi.org/10.1038/s43247-022-00489-4.
20. Park, S. W., Kim, J. S., and Kug, J. S. (2020). The intensification of Arctic warming as a result of CO_2 physiological forcing. Nat. Commun. *11*(1), 2098. https://doi.org/10.1038/s41467-020-15924-3.
21. Lemordant, L., and Gentine, P. (2019). Vegetation response to rising CO_2 impacts extreme temperatures. Geophys. Res. Lett. *46*(3), 1383-1392. https://doi.org/10.1029/2018GL080238.
22. Zhang, X., Alexander, L., Hegerl, G.C., Jones, P., Tank, A.K., Peterson, T.C., Trewin, B. and Zwiers, F.W. (2011). Indices for monitoring changes in extremes based on daily temperature and precipitation data. Wiley Interdiscip. Rev. Clim. Change. *2*(6), 851-870. https://doi.org/10.1002/wcc.147.
23. Mueller, B., and Seneviratne, S. I. (2012). Hot days induced by precipitation deficits at the global scale. PNAS *109*(31), 12398-12403. https://doi.org/10.1073/pnas.1204330109.
24. Li, Y., Piao, S., Li, L.Z., Chen, A., Wang, X., Ciais, P., Huang, L., Lian, X., Peng, S., Zeng, Z. and Wang, K. (2018). Divergent hydrological response to large-scale afforestation and vegetation greening in China. Sci. Adv. *4*(5), eaar4182. https://doi.org/10.1126/sciadv.aar4182.
25. Zeng, Z., Piao, S., Li, L.Z., Wang, T., Ciais, P., Lian, X., Yang, Y., Mao, J., Shi, X. and Myneni, R.B. (2018). Impact of Earth greening on the terrestrial water cycle. J. Clim. *31*(7), 2633-2650. https://doi.org/10.1175/JCLI-D-17-0236.1.
26. Lian, X., Piao, S., Li, L.Z., Li, Y., Huntingford, C., Ciais, P., Cescatti, A., Janssens, I.A., Peñuelas, J., Buermann, W. and Chen, A. (2020). Summer soil drying exacerbated by earlier spring greening of northern vegetation. Sci. Adv. *6*(1), eaax0255. https://doi.org/10.1126/sciadv.aax0255.
27. Donat, M.G., Alexander, L.V., Yang, H., Durre, I., Vose, R., Dunn, R.J., Willett, K.M., Aguilar, E., Brunet, M., Caesar, J. and Hewitson, B. (2013). Updated analyses of temperature and precipitation extreme indices since the beginning of the twentieth century: The HadEX2 dataset. J. Geophys. Res.: Atmos. *118*(5), 2098-2118. https://doi.org/10.1002/jgrd.50150.
28. Good, S. P., Noone, D., and Bowen, G. (2015). Hydrologic connectivity constrains partitioning of global terrestrial water fluxes. Science, 349(6244), 175-177. https://doi.org/10.1126/science.aaa5931.

29. Wei, Z., Yoshimura, K., Wang, L., Miralles, D. G., Jasechko, S., and Lee, X. (2017). Revisiting the contribution of transpiration to global terrestrial evapotranspiration. Geophys. Res. Lett. *44*(6), 2792-2801. https://doi.org/10.1002/2016GL072235.
30. Hirschi, M., Seneviratne, S.I., Alexandrov, V., Boberg, F., Boroneant, C., Christensen, O.B., Formayer, H., Orlowsky, B. and Stepanek, P. (2011). Observational evidence for soil-moisture impact on hot extremes in southeastern Europe. Nat. Geosci. *4*(1), 17-21. https://doi.org/10.1038/ngeo1032.
31. Yu, L., Liu, Y., Liu, T., and Yan, F. (2020). Impact of recent vegetation greening on temperature and precipitation over China. Agric. For. Meteorol. *295*, 108197. https://doi.org/10.1016/j.agrformet.2020.108197.
32. Wu, J., Wang, D., Li, L. Z., and Zeng, Z. (2022). Hydrological feedback from projected Earth greening in the 21st century. Sustainable Horizons, *1*, 100007. https://doi.org/10.1016/j.horiz.2022.100007.
33. Rahman, M. M., Lu, M., and Kyi, K. H. (2015). Variability of soil moisture memory for wet and dry basins. J. Hydrol. *523*, 107-118. https://doi.org/10.1016/j.jhydrol.2015.01.033.
34. Fischer, E. M., Seneviratne, S. I., Vidale, P. L., Lüthi, D., and Schär, C. (2007). Soil moisture–atmosphere interactions during the 2003 European summer heat wave. J. Clim. *20*(20), 5081-5099. https://doi.org/10.1175/JCLI4288.1.
35. De Kauwe, M.G., Medlyn, B.E., Zaehle, S., Walker, A.P., Dietze, M.C., Hickler, T., Jain, A.K., Luo, Y., Parton, W.J., Prentice, I.C. and Smith, B. (2013). Forest water use and water use efficiency at elevated CO_2: A model-data intercomparison at two contrasting temperate forest FACE sites. Global Change Biol. *19*(6), 1759-1779. https://doi.org/10.1111/gcb.12164.
36. Chen, C., Li, D., Li, Y., Piao, S., Wang, X., Huang, M., Gentine, P., Nemani, R.R. and Myneni, R.B. (2020). Biophysical impacts of Earth greening largely controlled by aerodynamic resistance. Sci. Adv. *6*(47), eabb1981. https://doi.org/10.1126/sciadv.abb1981.
37. Yu, L., Liu, Y., Yang, J., Liu, T., Bu, K., Li, G., Jiao, Y. and Zhang, S. (2022). Asymmetric daytime and nighttime surface temperature feedback induced by crop greening across Northeast China. Agr Forest Meteorol. *325*, 109136. https://doi.org/10.1016/j.agrformet.2022.109136.
38. Song, J., Wang, Z. H., Myint, S. W., and Wang, C. (2017). The hysteresis effect on surface-air temperature relationship and its implications to urban planning: An examination in Phoenix, Arizona, USA. Landscape Urban Plan. *167*, 198-211. https://doi.org/10.1016/j.landurbplan.2017.06.024.
39. Seneviratne, S. I., Donat, M. G., Mueller, B., and Alexander, L. V. (2014). No pause in the increase of hot temperature extremes. Nat. Clim. Change. *4*(3), 161-163. https://doi.org/10.1038/nclimate2145.
40. Fischer, E. M., and Schär, C. (2010). Consistent geographical patterns of changes in high-impact European heatwaves. Nat. Geosci. *3*(6), 398-403. https://doi.org/10.1038/ngeo866.
41. Center for International Earth Science Information Network - CIESIN - Columbia University. 2016. Gridded Population of the World, Version 4 (GPWv4): Population Count Adjusted to Match 2015 Revision of UN WPP Country Totals. Palisades, NY: NASA Socioeconomic Data and Applications Center (SEDAC). http://dx.doi.org/10.7927/H4SF2T42.
42. Herold, N., Alexander, L., Green, D., and Donat, M. (2017). Greater increases in temperature extremes in low versus high income countries. Environ. Res. Lett. *12*(3), 034007. https://doi.org/10.1088/1748-9326/aa5c43.
43. Buckley, L. B., and Huey, R. B. (2016). Temperature extremes: geographic patterns, recent changes, and implications for organismal vulnerabilities. Global Change Biol. *22*(12), 3829-3842. https://doi.org/10.1111/gcb.13313.

44. Cohn, A.S., Bhattarai, N., Campolo, J., Crompton, O., Dralle, D., Duncan, J. and Thompson, S. (2019). Forest loss in Brazil increases maximum temperatures within 50 km. Environmental Research Letters, *14*(8), 084047. https://doi.org/10.1088/1748-9326/ab31fb.
45. Knight, T., Price, S., Bowler, D., Hookway, A., King, S., Konno, K., and Richter, R. L. (2021). How effective is 'greening'of urban areas in reducing human exposure to ground-level ozone concentrations, UV exposure and the 'urban heat island effect'? An updated systematic review. Environ. Evid. *10*(1), 1-38. https://doi.org/10.1186/s13750-016-0054-y.
46. Ball, J. T., Woodrow, I. E., and Berry, J. A. (1987, October). A model predicting stomatal conductance and its contribution to the control of photosynthesis under different environmental conditions. In Progress in photosynthesis research: volume 4 proceedings of the VIIth international congress on photosynthesis providence, Rhode Island, USA, August 10–15, 1986 (pp. 221-224). Dordrecht: Springer Netherlands.
47. Leuning, R. (1995). A critical appraisal of a combined stomatal-photosynthesis model for C3 plants. Plant, Cell & Environment, *18*(4), 339-355. https://doi.org/10.1111/j.1365-3040.1995.tb00370.x.
48. Medlyn, B.E., Duursma, R.A., Eamus, D., Ellsworth, D.S., Prentice, I.C., Barton, C.V., Crous, K.Y., De Angelis, P., Freeman, M. and Wingate, L. (2011). Reconciling the optimal and empirical approaches to modelling stomatal conductance. Global Chang. Biol. *17*(6), 2134-2144. https://doi.org/10.1111/j.1365-2486.2010.02375.x.
49. Kosaka, Y., and Xie, S. P. (2013). Recent global-warming hiatus tied to equatorial Pacific surface cooling. Nature *501*(7467), 403-407. https://doi.org/10.1038/nature12534.
50. He, J., and Soden, B. J. (2016). The impact of SST biases on projections of anthropogenic climate change: A greater role for atmosphere-only models?. Geophys. Res. Lett. *43*(14), 7745-7750. https://doi.org/10.1002/2016GL069803.
51. Marti, O., Braconnot, P., Dufresne, J.L., Bellier, J., Benshila, R., Bony, S., Brockmann, P., Cadule, P., Caubel, A., Codron, F. and de Noblet, N. (2010). Key features of the IPSL ocean atmosphere model and its sensitivity to atmospheric resolution. Clim. Dyn. *34*, 1-26. https://doi.org/10.1007/s00382-009-0640-6.
52. Hourdin, F., Musat, I., Bony, S., Braconnot, P., Codron, F., Dufresne, J.L., Fairhead, L., Filiberti, M.A., Friedlingstein, P., Grandpeix, J.Y. and Krinner, G. (2006). The LMDZ4 general circulation model: climate performance and sensitivity to parametrized physics with emphasis on tropical convection. Clim. Dyn. *27*, 787-813. https://doi.org/10.1007/s00382-006-0158-0.
53. Krinner, G., Viovy, N., de Noblet-Ducoudré, N., Ogée, J., Polcher, J., Friedlingstein, P., Ciais, P., Sitch, S. and Prentice, I.C. (2005). A dynamic global vegetation model for studies of the coupled atmosphere-biosphere system. Glob. Biogeochem. Cycles. *19*(1). https://doi.org/10.1029/2003GB002199.
54. Harris, I., Osborn, T. J., Jones, P., and Lister, D. (2020). Version 4 of the CRU TS monthly high-resolution gridded multivariate climate dataset. Scientific data, 7(1), *109*. https://doi.org/10.1038/s41597-020-0453-3.
55. Hersbach, H., Bell, B., Berrisford, P., Hirahara, S., Horányi, A., Muñoz-Sabater, J., Nicolas, J., Peubey, C., Radu, R., Schepers, D. and Simmons, A. (2020). The ERA5 global reanalysis. Q. J. R. Meteorol. *146*(730), 1999-2049. https://doi.org/10.1002/qj.3803.
56. Fischer, E. M., and Knutti, R. (2015). Anthropogenic contribution to global occurrence of heavy-precipitation and high-temperature extremes. Nat. Clim. Change. *5*(6), 560-564. https://doi.org/10.1038/nclimate2617.